Ecological Engineering 97 (2016) 452–464

Contents lists available at ScienceDirect

Ecological Engineering

journal homepage: www.elsevier.com/locate/ecoleng

Effects of inset floodplains and hyporheic exchange induced by in-stream structures on nitrate removal in a headwater stream

Erich T. Hester[a,*], Benjamin Hammond[a], Durelle T. Scott[b]

[a] The Charles E. Via, Jr. Department of Civil and Environmental Engineering, Virginia Tech, 220-D Patton Hall, 750 Drillfield Drive, Blacksburg, VA 24061, United States
[b] Department of Biological Systems Engineering, Virginia Tech, 305 Seitz Hall, 155 Ag Quad Lane, Blacksburg, VA 24061, United States

ARTICLE INFO

Article history:
Received 24 May 2016
Received in revised form 30 July 2016
Accepted 5 October 2016
Available online 15 October 2016

Keywords:
Nutrients
Chesapeake Bay Program
Stream restoration
River restoration
Water quality
Total mass daily load (TMDL)

ABSTRACT

Stream restoration efforts in the United States are increasingly aimed towards water quality improvement, yet little process-based guidance exists to compare pollutant removals from different restoration techniques for variable site conditions. Excess nitrate (NO_3^-) is a frequent pollutant of concern due to eutrophication in downstream waterbodies such as the Chesapeake Bay. We used MIKE SHE to simulate hydraulics and NO_3^- removal in a 90 m restored reach of Stroubles Creek, a second-order stream in Blacksburg, Virginia. Site specific geomorphic, hydrologic, and hydraulic data were used to calibrate the model. We evaluated in-stream structures that induce hyporheic zone denitrification during baseflow and inset floodplains that remove NO_3^- during storm flows. We varied hydraulic conditions (winter baseflow, summer baseflow, storm flow), biogeochemical parameters (literature hyporheic zone denitrification rates and newly available inset floodplain removal rates) and boundary conditions (upstream NO_3^- concentration), sediment conditions (hydraulic conductivity), and stream restoration design parameters (inset floodplain length). Our results indicate that NO_3^- removal rates within the 90 m reach were minimal. Structure-induced hyporheic zone denitrification did not exceed 3.1% of mass flowing in from the upstream channel, was achieved only during favorable background groundwater hydraulic conditions (i.e. summer baseflow), and was transport-limited such that non-trivial removal rates were achieved only when the streambed hydraulic conductivity (K) was at least 10^{-4} m/s. Inset floodplain nitrogen removal was limited by floodplain residence time and NO_3^- removal rate, and did not exceed 1% of inflowing mass. Summing these removals for both restoration practices over the course of the year based on the frequency of storm and summer baseflow conditions yielded ~2.1% annual removal. Achieving 30% NO_3^- removal required increasing the length of stream reach restored to 0.9 km–819 km (depending on hydraulic conductivity) and 3.8–46 km (depending on inset floodplain length and nitrogen removal rate) for in-stream structures during baseflow and inset floodplains during storm flow, respectively. In one of the first comparisons of process-based modeling to the Chesapeake Bay Program stream restoration guidance, we found that the guidance overestimated hyporheic NO_3^- removal for our modeled reach, but correctly estimated inset floodplain removal. Overall, our results indicate that in-stream structures and inset floodplains can improve water quality, but overall required level of effort may be high to achieve desired results.

1. Introduction

1.1. Excess nitrogen and stream restoration

Excess nitrogen (N) loading is caused by anthropogenic activity, especially nitrate (NO_3^-) fertilizer runoff from agriculture (Royer et al., 2006). Downstream movement of N is then accelerated by channel incision and simplification from reduced storm infiltration in the contributing watershed (Henshaw and Booth, 2000), which reduces residences times and hence potential for natural attenuation. As a result, a high amount of N reaches coastal waters, causing problems associated with eutrophication (Howarth et al., 2002). In the Chesapeake Bay, nutrient loading has caused hypoxia and algal blooms (Kemp et al., 2005) and has negatively affected the ecosystem (Langland et al., 2000), leading to the monumental Chesapeake Bay Total Maximum Daily Load (TMDL) for N, phosphorous (P) and sediment (USEPA, 2010).

* Corresponding author.
E-mail addresses: ehester@vt.edu (E.T. Hester), hammondb@vt.edu (B. Hammond), dscott@vt.edu (D.T. Scott).

http://dx.doi.org/10.1016/j.ecoleng.2016.10.036
0925-8574/

Stream restoration aims to return stream corridors toward a preferable former condition, adapt them to a new environment, and/or control the factors adversely affecting the river (Brookes and Shields, 1996; Downs and Gregory, 2004; Wohl et al., 2005, 2015; Landers, 2010; Palmer et al., 2014). Many stream restoration practices are considered for mitigating water quality impacts, including channel realignment, riparian planting, in-stream structure installation, and floodplain reconnection (Roni et al., 2002; Ensign and Doyle, 2005; Kaushal et al., 2008; Opperman et al., 2009; Hester and Gooseff, 2010; Mason et al., 2012; Azinheira et al., 2014; Johnson et al., 2015; Jones et al., 2015). Yet water quality improvement is a relatively new goal compared to more traditional objectives such as bank stabilization, ecosystem enhancement or riparian zone management (Bernhardt et al., 2005), and little guidance is available to guide stream restoration design for purposes of improving N removal from the channel (Craig et al., 2008; Veraart et al., 2014; Johnson et al., 2015).

The Chesapeake Bay Program recently issued protocols that quantify the water quality benefits of stream restoration schemes and offer mitigation credits for strategies that prevent sediment erosion during storm flows, promote hyporheic zone nutrient processing, reconnect stream channels to their floodplains, and/or capture nutrient/sediment-laden runoff in upland dry channels (Berg et al., 2014). These protocols are a substantial advance in that they are the first to give varying water quality credit depending on which broad category of stream restoration practice is implemented. Yet the protocols do not acknowledge variability of water quality results within each category based on different specific practices (e.g., in-stream structures versus meanders), or in different specific settings (e.g., watershed position, geologic substrate), and are based on a small list of field studies (Jordan, 2007; Kaushal et al., 2008; Striz and Mayer, 2008). Expanding the range of information regarding the potential for stream restoration practices to impact water quality thus will be beneficial.

1.2. Hydraulic connection and residence time in storage zones

Stream restoration strategies enhance water quality by promoting the conditions that cause natural pollutant attenuation. When N removal is sought, these conditions are characterized by long contact times between N-impacted water and sediments or soils with high denitrification potential (Roley et al., 2012b). These conditions are typically achieved by exchange with off-channel storage zones where water moves more slowly than in the channel. In-stream structures achieve these conditions by inducing backwater upstream of the structure, which drives pollutants temporarily into streambed sediments (i.e. hyporheic zone, Hester and Doyle, 2008; Hester and Gooseff, 2010). Given favorable microbial and redox conditions (i.e. an anoxic environment with sufficient labile organic carbon), NO_3^- may be removed by denitrification in the subsurface before upwelling downstream of the structure (Kasahara and Hill, 2006; Lautz and Fanelli, 2008; Zarnetske et al., 2011). Inset floodplains (i.e. floodplain benches installed lower than top of bank) achieve N removal by promoting contact between N-laden water and plants and organic material as water moves across the inset floodplains at relatively low velocities (Roley et al., 2012a,b; Azinheira et al., 2014). This is also achieved by bankfull floodplains by a similar principle (Kaushal et al., 2008; Jones et al., 2015).

The efficacy of such N removal is controlled by the connectivity between the main channel and the reactive storage zone(s), the residence time distribution in the storage zone(s), and the strength of the removal mechanism (i.e. reaction or removal rate) (Stewart et al., 2011), such that ultimately one of these factors will limit the rate of N removal. Identification of this limiting factor on a strategy-specific and even site-specific basis will help to quantify the cost of achieving meaningful water quality improvements through stream restoration.

1.3. Objectives of study

The purpose of this study was to investigate the effectiveness of inset floodplains and in-stream structures at removing NO_3^- from a 90 m restored reach of Stroubles Creek in Blacksburg, Virginia. We used MIKE SHE to estimate removal as the percent of upstream NO_3^- that is removed via hyporheic zone denitrification during baseflow and inset floodplain NO_3^- removal during storm flow. Our specific objectives were to 1) determine the relative importance of various controls (e.g., sediment hydraulic conductivity, denitrification rates, stream restoration design parameters) on reach-scale steady-state NO_3^- removal using a rigorous process-based approach, 2) estimate net removal over the course of a year subject to natural seasonal variations in hydraulic boundary conditions, 3) determine the length of restored reach required for water quality improvement to become substantial, and 4) compare our modeled NO_3^- removal to those predicted by the Chesapeake Bay Program protocols in Berg et al. (2014).

2. Methods

2.1. Model governing equations

We used MIKE SHE (Graham and Butts, 2005; DHI, 2011) to model surface water and groundwater hydraulics, and dissolved solute transport with reaction in a stream reach, including surface water-groundwater interaction. We extended a previously developed MIKE SHE model of surface water-groundwater hydraulics and conservative tracer transport (Azinheira et al., 2014) in a stream reach located near Blacksburg, Virginia. MIKE SHE uses a fully implicit three-dimensional finite difference algorithm to solve the groundwater flow equation and an explicit algorithm to solve the two-dimensional diffusive wave approximation of the Saint Venant equation for surface water (Graham and Butts, 2005). Additional detail on the equations of the hydraulic model can be found in Azinheira et al. (2014).

The water quality component of MIKE SHE simulates solute transport using the advection-dispersion equation:

$$\frac{\partial C}{\partial t} = \frac{\partial}{\partial x_i}(cv_i) + \frac{\partial}{\partial x_i}\left(D_{ij}\frac{\partial C}{\partial x_j}\right) + R_c + \left(\frac{\partial C}{\partial t}\right)_{reactions} \quad (1)$$

where C is the concentration of the dissolved solute in the model cell (g/m^3), t is time (s), $x_{i,j}$ is the distance along the respective Cartesian coordinate axis (m), v_i is the velocity vector determined during the hydraulics simulation (m/s), D_{ij} is the dispersion tensor (m^2/s), and R_c is the sum of the sources and sinks (g/m^3-s). MIKE SHE uses the three-dimensional (i,j = 1,2,3) advection-dispersion equation for solute transport in groundwater and the two-dimensional advection-dispersion equation (i,j = 1,2) for solute transport in surface water.

MIKE SHE also allows chemical reaction processes that remove solute from saturated groundwater and/or surface water. We simulated denitrification in the hyporheic zone and N removal in the inset floodplains by assuming first-order decay of NO_3^-, which can vary in space:

$$\left(\frac{\partial C}{\partial t}\right)_{reactions} = -kC \quad (2)$$

where k is the first-order decay rate (s^{-1}). MIKE SHE solves the advection-dispersion equation using the QUICKEST method (Leonard, 1979), an explicit scheme that applies upstream and

central differencing for the advection and dispersion terms, respectively (DHI, 2011). Denitrification in hyporheic zone models is often simulated as Michaelis-Menten (Monod) kinetics (Gu et al., 2007, Zarnetske et al., 2012), however first-order kinetics are justified when the NO_3^- concentration is less than the reaction half-saturation constant of 1.64 mg/L NO_3^-N (Boyer et al., 2006; Stewart et al., 2011; Zarnetske et al., 2012, 2015; Harvey et al., 2013). We used a base case NO_3^- concentration of 1.0 mg/L NO_3^-N, thus we were below this threshold during most of our model runs. However, we did vary influent NO_3^- concentration up to 3.0 mg/L during the sensitivity analysis (Section 2.2.4). Our first-order approximation may have overestimated denitrification at this concentration, and we discuss implications of this in the discussion.

2.2. Model setup

2.2.1. Study site

The study site is the same 90 m long reach containing four meanders described by Azinheira et al. (2014). It is part of a 1.5 km restored segment of Stroubles Creek, a third-order stream in Blacksburg, Virginia. Restoration was completed in 2010 and involved inset floodplain installation, riparian zone planting, and bank stabilization (Wynn et al., 2010). There are currently no in-stream structures in the reach. The land use that contributes hydrologically to the stream reach is both urban and agricultural. More details are given in Azinheira et al. (2014).

2.2.2. Hydraulic parameters and boundary conditions

The existing hydraulic model, including grid discretization, incorporation of existing groundwater and surface water data, site topography, and groundwater/surface water hydraulic properties, is identical to that described by Azinheira et al. (2014) except where noted below. Briefly, the model domain was 100 m long in the downstream direction and 75 m laterally, and 5 m vertically into groundwater with 102 columns, 77 rows, and 25 layers for 7850 total computational nodes. The channel slope averaged 0.0023 m/m, the channel width averaged 3.5 m, and inset floodplains averaged 3.0 m wide.

As in Azinheira et al. (2014), surface water flows and groundwater boundary conditions were based on field measurements at the site. The summer baseflow in the modeled stream reach was 0.025 m^3/s with a depth of 0.1 m at the thalweg, and the winter baseflow was 0.059 m^3/s with a depth of 0.15 m at the thalweg. Groundwater boundary heads also varied with the seasons. The simulated storm flow was 1.7 m^3/s with flow depths of 0.65 m and approximately 0.15 m at the thalweg and in the inset floodplains, respectively.

We varied seasonal hydraulic conditions (channel flow and groundwater boundary heads), hydraulic conductivity of sediment, and the Manning's roughness coefficient (n) as part of the sensitivity analysis (Section 2.2.4). The only difference with Azinheira et al. (2014) was that for summer baseflow we varied hydraulic conductivity up to $K = 10^{-3}$ m/s (rather than $K = 10^{-4}$ m/s) which is a relatively high but feasible streambed conductivity value (Calver, 2001; Menichino and Hester, 2014). This was to investigate hyporheic denitrification when there is relatively high hydraulic connection between the main channel and the hyporheic zone.

We simulated two in-stream structures (weirs) in the 90 m reach that represent common in-stream restoration structures such as boulder weirs, log dams, w-weirs, upstream v's, and cross vanes (Doll et al., 2003; Roni et al., 2006; NRCS, 2007; Hester and Doyle, 2008; Lautz and Fanelli, 2008; Gordon et al., 2013). Each structure was 1 m long (thick) in the direction of flow, 3 m long perpendicular to the flow, and each extended 0.3 m above the streambed and approximately 0.2 m (one computational layer) into the streambed (Azinheira et al., 2014). These structures were spaced 45 m apart consistent with restoration guidance and prior research for a stream of this discharge (Rosgen, 2001; Crispell and Endreny, 2009; Buchanan et al., 2012; Azinheira et al., 2014).

We simulated off-channel storage during storm flows using four inset floodplains in the 90 m reach. We varied the individual inset floodplain length during sensitivity analysis (Section 2.2.4); the minimum and maximum cases were L = 0 (no inset floodplains) and L = Full (inset floodplain installation along both banks of the entire stream reach). We implemented the inset floodplains by altering the model topography, as described by Azinheira et al. (2014). We generalized the floodplain length using the parameter F_b, which represents the percentage of the stream reach length with inset floodplains.

2.2.3. Transport parameters and boundary conditions

2.2.3.1. Hyporheic zone denitrification rates. We simulated hyporheic zone NO_3^- removal via denitrification by assigning a first-order decay rate to the groundwater component of the model. While hyporheic zone denitrification can be simulated following Michaelis-Menten kinetics (Cardenas et al., 2008; Marzadri et al., 2011; Kessler et al., 2015), models using first-order kinetics have been successfully calibrated to field data (Boyer et al., 2006; Stewart et al., 2011; Harvey et al., 2013; Zarnetske et al., 2015), and it is considered reasonable to simulate it as a first order process when NO_3^- concentrations are low (Sheibley et al., 2003; Marzadri et al., 2011; Gu et al., 2012), which they are in this case. We varied this parameter in our sensitivity analysis using a range of literature values (Section 2.2.4, Table 1).

We did not model nitrification but acknowledge that it may also occur in the saturated zone under aerobic conditions. Our approach is consistent with prior studies (Gu et al., 2012; Hester et al., 2014), and is justified because the relatively low K values for most of the model scenarios (10^{-4}–10^{-8} m/s) result in long residence times, such that only a very small percentage of most hyporheic flowpaths would be considered nitrification zones (Zarnetske et al., 2011; Marzadri et al., 2012). In other words, oxygen would be used up by aerobic metabolism and nitrification relatively quickly at the beginning of each hyporheic flowpath, and then conditions would be conducive to denitrification thereafter. For example, at $K = 10^{-4}$ m/s, nitrification would be possible in approximately 3% of the hyporheic zone volume induced by the structures in our model based on the hyporheic zone residence times calculated for those hyporheic zones by Azinheira et al. (2014) and the net nitrification/denitrification threshold of 7.5 h proposed by Zarnetske et al. (2011). For all lower K's used in our sensitivity analysis ($K = 10^{-5}$ m/s, 10^{-6} m/s, 10^{-7} m/s, and 10^{-8} m/s, Table 1), the percentage would be even smaller. At our highest K (10^{-3} m/s), residence times are expected to be approximately ten times shorter than those observed at $K = 10^{-4}$ m/s, meaning that approximately 30% of most hyporheic flowpaths would be considered nitrification zones. For simplicity, these nitrification zones were not considered and the entire saturated zone was assigned a uniform first-order denitrification rate based on rates gathered from modeling studies in the literature (Table 1). The results of the $K = 10^{-3}$ m/s simulations may overestimate the net removal of NO_3^- within the modeled stream reach.

2.2.3.2. Inset floodplain nitrate removal rates. Floodplain NO_3^- loss occurs by denitrification in shallow sediment/organic matter and uptake by plants (Roley et al., 2012a,b; Jones et al., 2015). We simulated N removal by assigning a first-order removal rate in the surface water model cells directly above the inset floodplains. Within each model run the removal rate was the same for all four of the inset floodplains. There were no reactions in the main channel. We identified inset floodplain surface water cells as every cell where the flow depth was less than 18 cm (Fig. 1). We chose

Table 1
Baseflow model scenarios.

Parameter	Description	Base Case	Minimum	Maximum	Presence of Structures
Groundwater Hydraulic Boundaries	Summer baseflow Winter baseflow	Summer baseflow			Run with and without structures
Sediment Hydraulic Conductivity (K)	Varied from that of a coarse sand to a silty-clay	10^{-6} m/s	10^{-8} m/s	10^{-3} m/s	Run with structures only
Influent NO_3^- Concentration	Varied across typical range for mixed land-use[a]	1 mg/L NO_3^-N	0.5 mg/L NO_3^-N	3 mg/L NO_3^-N	Run with structures only
Saturated Zone Decay Rate	Varied across range collected from literature[b]	6 d^{-1}	0.6 d^{-1}	36 d^{-1}	Run with structures only

[a] NO_3^- concentrations from Dubrovsky et al. (2010).
[b] Values from Sheibley et al. (2003), Gu et al. (2007), Marzadri et al. (2011), and Zarnetske et al. (2012).

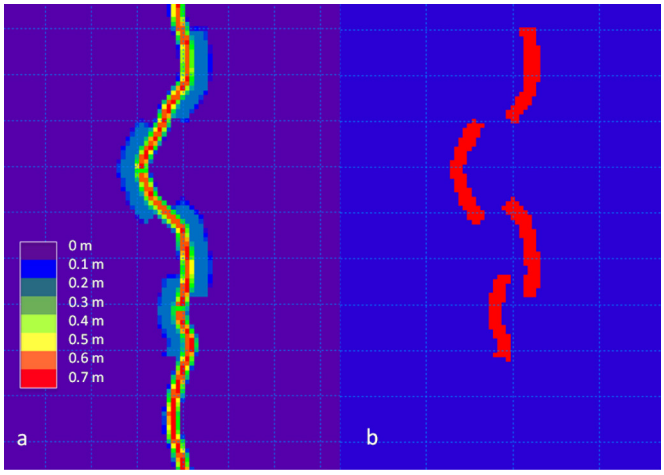

Fig. 1. Plan view of (a) model flow depths during storm flow conditions, and (b) areas (shown in red) assigned a surface water first-order decay rate for example inset floodplains scenario with L = 20 m (Table 2) (For interpretation of the references to color in this figure legend, the reader is referred to the web version of this article.).

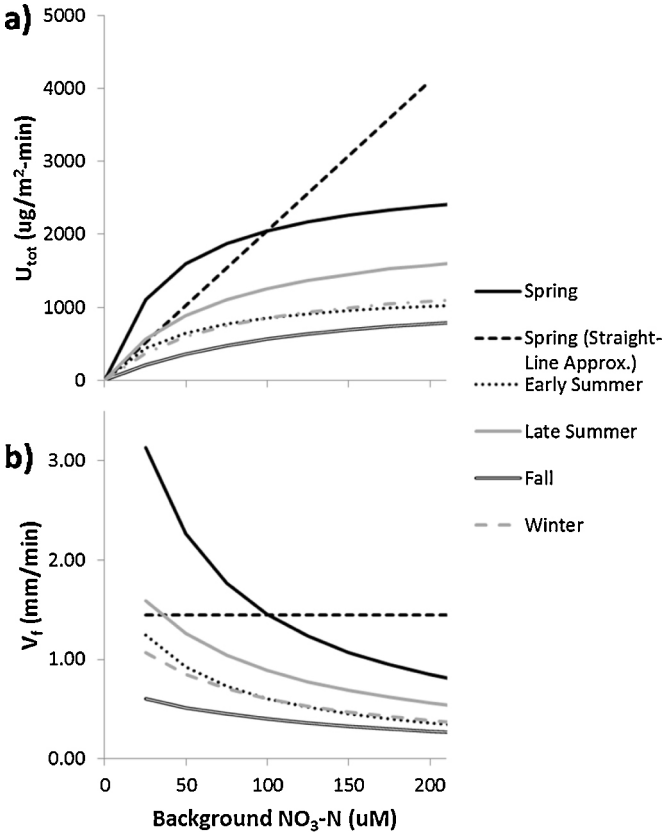

Fig. 2. Areal N uptake rates (U_{tot}) plotted against background NO_3^- concentration (a) using the Michaelis-Menten constants developed by Jones et al. (2015); we fitted straight lines from the origin through each seasonal dataset (example shown for Spring) to calculate a range of first-order decay rates. Uptake velocity (V_f, i.e. U_{tot} divided by background NO_3^- concentration) plotted against background NO_3^- concentration (b); the example straight-line approximation from panel a is shown again; this value (1.45 mm/min) is divided by the inset floodplain water depth (150 mm) and used as the maximum first-order N removal rate (14.0 d^{-1}).

this number to capture the cells with steady-state flow depths of approximately 15 cm (representing most of the inset floodplain cells), as well as those on the floodplain banks (with even shallower flow) and some of the cells nearer the channel with slightly greater depths that were located mostly in the inset floodplain and only partially in the main channel.

We calculated the first-order removal rate for NO_3^- uptake above the inset floodplains using nutrient spiraling parameters from the field study Jones et al. (2015). That field study occurred in the same reach of Stroubles Creek as we simulate here, and to our knowledge is the first time carbon, N, and P dynamics have been measured in controlled experimental overbank floods in a short-residence time (i.e. headwater) riparian floodplain (Jones et al., 2015). Jones et al. (2015) provides areal uptake rates that follow Michaelis-Menten kinetics and therefore relate nonlinearly to NO_3^- concentration. We extracted first-order rate constants (i.e. where the rate relates linearly to NO_3^- concentration) that approximate the Michaelis-Menten kinetics at relatively low NO_3^- concentrations.

We divided the areal NO_3^- uptake rates (U_{tot}, mg NO_3^-N min^{-1} m^{-2}) from Jones et al. (2015) (Fig. 2a) by the corresponding background NO_3^- concentrations (mg NO_3^-N L^{-1}) by fitting straight lines from the origin to its respective Michaelis-Menten plot at 100 μM (1.4 mg/L) NO_3^-N (Fig. 2a–b). This particular background concentration was chosen because it is near the base case NO_3^- concentration (1 mg/L, Tables 1–2). This approach overestimates NO_3^- removal at background NO_3^- concentrations above 1.4 mg/L (i.e. 2 mg/L and 3 mg/L) and underestimates NO_3^- removals at lower background concentrations (i.e. 1 mg/L and 0.5 mg/L), though it represents the Michaelis-Menten rates at 1 mg/L and 2 mg/L fairly closely. We divided each resulting V_f by the steady-state water depth (m) in the modeled inset floodplain to establish a range of first-order NO_3^- uptake rates (min^{-1}) (Ensign and Doyle, 2006) (Table 2).

These values quantified the net effect of all processes that remove NO_3^-, including denitrification in shallow sediment/organic matter and uptake by plants. They provide suitable estimates of V_f for this study because they were developed between the inlet and outlet of a floodplain, rather than across an entire stream reach (where one would expect less N uptake per unit area and time). This was desirable for this study, because the rates were applied only to the inset floodplains and not to the main channel.

Table 2
Storm flow model scenarios.

Parameter	Description	Base Case	Minimum	Maximum	Presence of Structures
Inset Floodplain Length	Varying the percentage of the stream with inset floodplains	20 m (F_b = 0.44)	0 m (F_b = 0)	90 m (F_b = 1)	Run with structures only
NO_3^- Removal Rate	Varied using range collected by Jones et al. (2015)	5.8 d^{-1}	3.8 d^{-1}	14.0 d^{-1}	Run with structures only
Influent NO_3^- Concentration	Varied across typical range for mixed land-use	1 mg/L NO_3^-N	0.5 mg/L NO_3^-N	3 mg/L NO_3^-N	Run with structures only
Manning's Roughness Coefficient (n)	Varied in inset floodplains	0.07	0.5	1	Run with structures only

2.2.4. Model base case and sensitivity analysis

In order to determine the relative importance of various controls on NO_3^- removal, we varied the hydraulic boundaries, streambed hydraulic conductivity, inset floodplain length, influent NO_3^- concentration, first-order hyporheic zone denitrification rate, and first-order inset floodplain NO_3^- removal rate in our sensitivity analysis on a one-at-a-time basis relative to a base case. We also varied Manning's roughness coefficient (n) in the inset floodplain during storm flow (Tables 1–2).

We varied influent boundary NO_3^- concentrations from 0.5 mg/L to 3 mg/L (all NO_3^- concentrations expressed as N) in a sensitivity analysis, as a typical range for mixed land-use streams (Dubrovsky et al., 2010). We accomplished this in the model using a mass flowrate injection into the boundary cells, where we set the mass flowrate amount to give the desired concentration in the cells immediately downstream from the injection point. We also injected a conservative tracer where everything was identical to the NO_3^- (e.g., injection locations, mass flowrates) except that no reaction occurred. The injection rates remained constant with time.

2.3. Model output

We assessed each model scenario in terms of percentage of inflowing NO_3^- removed by reactive loss within the reach, and in some cases total mass removed. We calculated this using the MIKE SHE mass balance output function, which gives the mass of solute added to and removed from the model over a user-specified timeframe (every hour for the storm flow models, which reached steady state very quickly, and every 48 h for the baseflow models). These values are further broken down between surface water and groundwater. For example, we assessed the storm flow scenarios based on the mass removed from the surface water by first-order decay. Similarly, we assessed the baseflow models based on the mass removed from the saturated zone.

We calculated the percentage NO_3^- removal for each model scenario by dividing the amount removed by the amount added to the upstream end of the channel. Model scenarios were run to steady-state, which we identified for the baseflow simulations as when the amount of the NO_3^- stored in the model (in grams) became constant to six significant digits (the default MIKE SHE precision) from one 48-h time period to the next. The storm flow scenarios were run for one hour of model time, which was sufficient for the surface water NO_3^- storage to stabilize to four significant digits over the course of ten minutes (e.g. 441.30 g at t = 45 min; 441.31 g at t = 55 min); typically the amount of NO_3^- stored in the surface water reached 99% of the steady-state value within four minutes.

There were no other NO_3^- sources in the model besides the upstream surface water boundary. The groundwater did not contain an initial concentration of NO_3^-, thus all NO_3^- appearing in the groundwater during the model runs had migrated from the channel as a result of hyporheic exchange or gross losing. This arrangement allows the model to quantify only removal of NO_3^- moving downstream in surface water from the contributing watershed. In other words, we are quantifying the NO_3^- removal effect that structures and inset floodplains have by inducing exchange from the channel into slower-moving off-channel zones. On the other hand, groundwater without NO_3^- would upwell into the channel due to gross gaining or structure-induced hyporheic exchange where hyporheic residence times were long enough for NO_3^- decay to be complete, causing NO_3^- concentrations in the channel to decrease due to dilution. Given this situation, we avoided overestimating NO_3^- removal by measuring the actual denitrified mass rather than the downstream NO_3^- concentration. Finally, there was no additional injection of NO_3^- to the overland flow to simulate local runoff within the stream reach. Though groundwater and local runoff would normally be expected to contribute NO_3^- to the system, they were ignored in order to isolate the reach-scale effects of in-stream structures and inset floodplains on removal of NO_3^- moving down the channel from upstream areas.

3. Results

3.1. Nitrate concentrations in space and time

During both storm flow and summer baseflow scenarios, only small reductions in surface water NO_3^- concentrations were observed between the upstream and downstream model boundaries (Fig. 3). The maximum reduction among the storm flow scenarios was for full (continuous, F_b = 1) inset floodplains (Fig. 3, left) where surface water NO_3^- concentrations decreased from 1 mg/L NO_3^-N at the upstream boundary to 0.98 mg/L NO_3^-N at the downstream boundary. In the storm flow simulations, steady-state NO_3^- concentrations were lower above the inset floodplains than in the main channel, typically dropping to 0.96–0.99 mg/L depending on the first-order removal rate.

The maximum NO_3^- concentration reduction among the baseflow scenarios was the summer baseflow model using K = 10^{-3} m/s (Fig. 3, right), due partially to hyporheic zone denitrification and partially to upwelling of groundwater that did not contain NO_3^-. In this case, the surface water NO_3^- concentrations decreased from 1.00 mg/L NO_3^-N at the upstream end of the channel to 0.84 mg/L NO_3^-N at the downstream end. By comparison, the conservative tracer concentrations decreased to 0.86 mg/L, indicating that most of the drop in NO_3^- concentration was due to dilution with groundwater.

Hyporheic exchange was induced by the in-stream structures only during summer baseflow. Under these conditions, shallow steady-state (late time) groundwater NO_3^- concentrations immediately upstream of the in-stream structures were similar to the influent surface water concentration. At greater hydraulic conductivities, elevated NO_3^- concentrations were also observed in the subsurface beneath the in-stream structures (e.g., K = 10^{-3} m/s, Fig. 4). Upwelling of NO_3^- downstream of the in-stream structure was observed only at the highest hydraulic conductivity and the lowest decay rate (Fig. 4a), as the residence time was insufficient to remove all of the NO_3^- (reaction limited). At higher decay rates (Fig. 4b and c) there is very little upwelling of NO_3^-, and removal is instead limited by the rate of NO_3^- (and hence water)

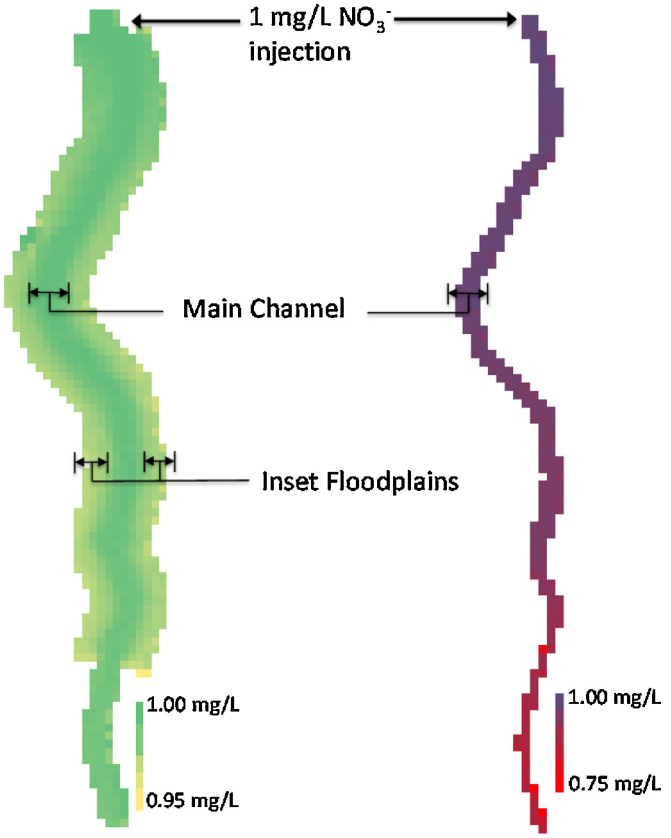

Fig. 3. Plan view concentration maps of top model layer (surface water) of the 90 m reach for example storm flow (left) and summer baseflow (right) scenarios. These are the conditions that caused the greatest observed NO_3^- removals (i.e. full-bank floodplain implementation and maximum removal rate for the storm flow, hydraulic conductivity $K = 10^{-3}$ m/s and maximum hyporheic zone denitrification rate for the baseflow) (For interpretation of the references to color in this figure legend, the reader is referred to the web version of this article.).

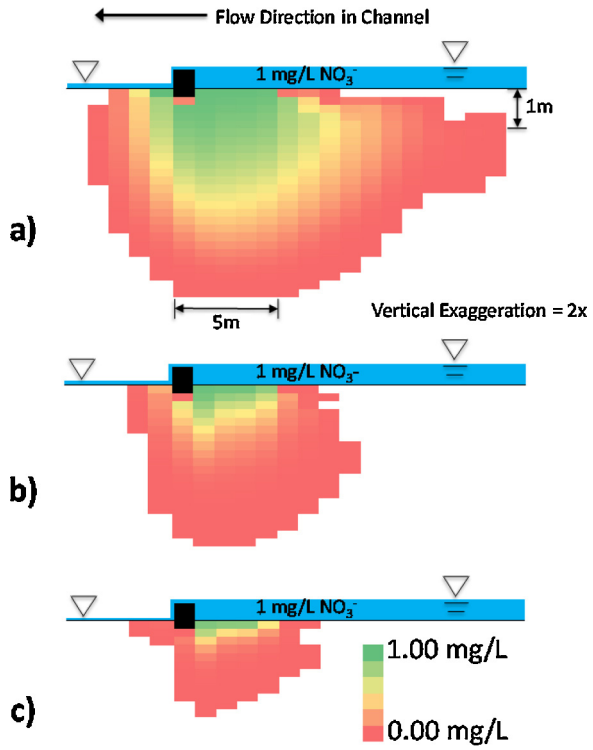

Fig. 4. Longitudinal section view concentration maps of the hyporheic zone at steady state (late time) during summer baseflow at the maximum hydraulic conductivity of $K = 10^{-3}$ m/s and first-order decay rates of (a) $k = 0.6\,d^{-1}$, (b) $k = 6\,d^{-1}$, and (c) $k = 36\,d^{-1}$. Shown in color are cells that contain NO_3^-N at concentrations greater than 1×10^{-5} mg/L. Surface water is shown schematically (i.e. not to scale) in blue. The black filled rectangles are the in-stream structure. (For interpretation of the references to color in this figure legend, the reader is referred to the web version of this article.)

exchange from the channel to the saturated zone (transport limited). In the models with hydraulic conductivities of $K = 10^{-5}$ m/s and lower, NO_3^- did not appear beneath the in-stream structures at non-negligible concentrations because the solute was removed very early in the hyporheic flow path (i.e. almost immediately after entering the subsurface), regardless of the first-order decay rate.

As found by Azinheira et al. (2014), channel residence times of NO_3^-/tracer were shortest during storm flows, which were unaffected by the presence of in-stream structures (Fig. 5 a). Channel residence times were longer for summer baseflow than for winter baseflow, and they were longer with in-stream weirs than without in-stream weirs during both baseflow conditions. Inset floodplain residence times increased with inset floodplain length (Fig. 5b–c). Hyporheic residence times were very sensitive to changes in sediment K (Fig. 5d). At the maximum K (10^{-3} m/s), the downstream upwelling cell reached its steady-state concentration within a few days, whereas at $K = 10^{-6}$ m/s the upwelling cell had not yet reached 20% of the steady-state concentration after 90 days.

The NO_3^- breakthrough curves were visually indistinguishable from the conservative tracer breakthrough curves at the downstream end of the stream reach for most of the storm flow simulations because little NO_3^- was removed due to short inset floodplain residence times (Fig. 5a). By contrast, the NO_3^- breakthrough curves within the inset floodplains where water flowed back into the main channel did show reductions, albeit small, relative to the conservative tracer (Fig. 5b and c) due to NO_3^- uptake in the inset floodplains. Finally, NO_3^- breakthrough did not occur at the upwelling end of hyporheic flowpaths induced by the in-stream structures (i.e. where water flowed back into the channel) during most of the summer baseflow simulations (Fig. 5d) due to substantial consumption by denitrification in the hyporheic zone. The exception was for the highest sediment K simulated (10^{-3} m/s), where NO_3^- upwelled at a steady-state concentration of 0.25 mg/L (using the base case first-order decay rate of $6\,d^{-1}$) compared to the steady-state tracer concentration of approximately 1 mg/L.

3.2. *Baseflow nitrate removal by structure-induced hyporheic flow*

Under summer baseflow conditions, the in-stream structures induced hyporheic flow but the inset floodplains were not engaged. Under these conditions we observed a tenfold increase in percent inflowing NO_3^- removed within the reach with each corresponding tenfold increase in hydraulic conductivity to a maximum of 2.8% (Fig. 6a) at the base case first-order decay rate. Percent removal rates at the lower hydraulic conductivities were completely negligible because the rates of hyporheic exchange of water were very low relative to the flow rate in the channel. Removal varied linearly with hydraulic conductivity between $K = 10^{-7}$ and $K = 10^{-4}$ m/s, as hyporheic zone residence times were long enough that nearly all of the NO_3^- entering the saturated zone was removed before reentering the channel. NO_3^- removal in these conditions is thus transport limited.

At $K = 10^{-4}$ m/s, NO_3^- removal starts to become reaction or kinetics limited (see subtle break in linearity, Fig. 6a), as NO_3^- mass moves quickly enough through the hyporheic zone that not all is removed. Under these conditions, increasing the first-order decay

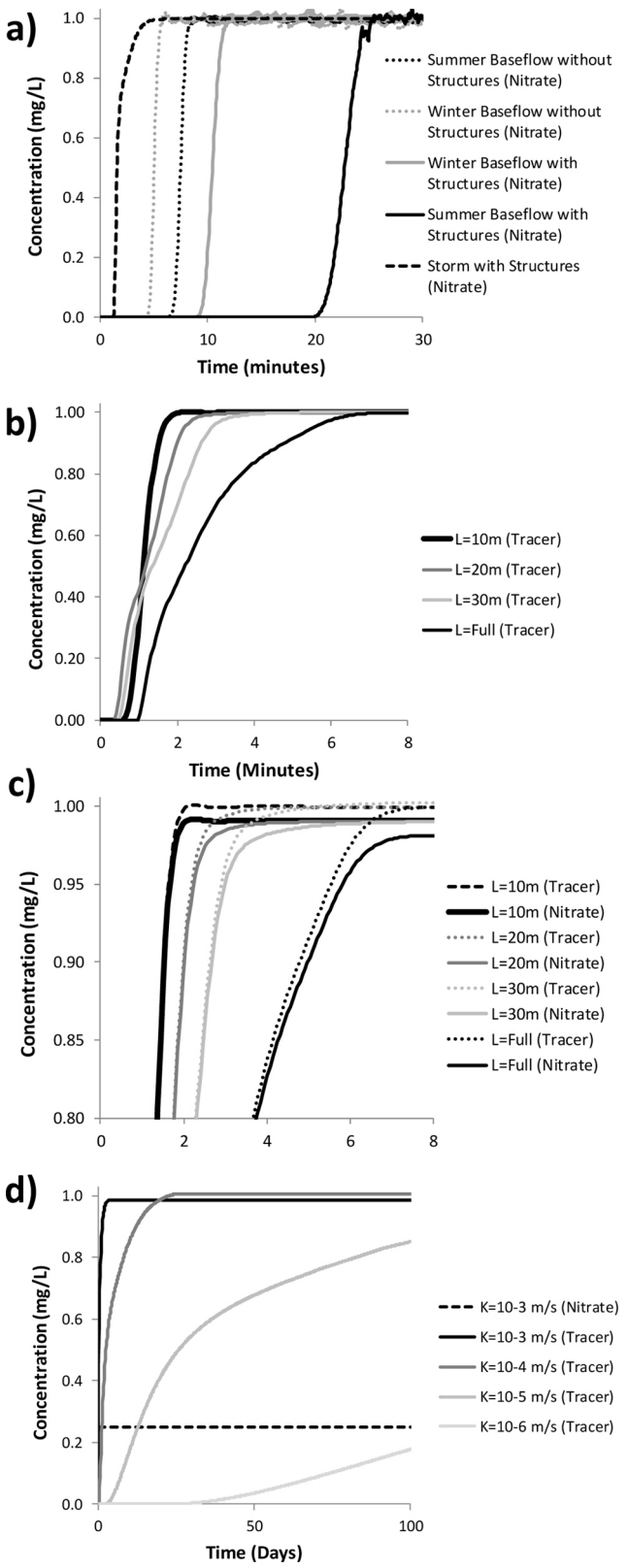

Fig. 5. Breakthrough curves in a) the channel at the downstream model boundary for various flow conditions, b) the upstream-most inset floodplain where it exits back to the channel during storm flow conditions, c) same as panel b but zoomed in axes to show fine distinctions, and d) the hyporheic zone at upwelling cell 1 m downstream of the in-stream structure (i.e. where hyporheic water exits back to water column) during summer baseflow conditions. For a) and b), conservative tracer breakthrough curves are not shown separately from NO_3^- breakthrough curves because they are visually indistinguishable in all cases because of how little NO_3^- is removed. For b) and c), location of breakthrough curve is the center of mass flux exiting the inset floodplain. L is the individual inset floodplain length and L = Full indicates full (continuous) inset floodplain installation on both banks. Center of mass flux locations were identified by Azinheira et al. (2014). NO_3^- removal rates were 14 d^{-1} above the inset floodplains in a), b), and c), and 6 d^{-1} in saturated groundwater in d).

rate increases the percent removal achieved, for example increasing from 2.0% to 3.1% at K = 10^{-3} m/s when the first-order decay rate was varied from its minimum (0.6 d^{-1}) to its maximum (36 d^{-1}) as shown in the top line in Fig. 6b. However, when decay rate increases yet further, i.e. beyond 36 d^{-1} (rightmost point on K = 10^{-3} m/s line in Fig. 6b), removal again becomes transport-limited because the reaction rate is so high that it is consuming all the NO_3^- that is provided by transport from surface water. By contrast, for K = 10^{-6} m/s, removal is entirely transport limited and there is no benefit from increasing the decay rate beyond the minimum 0.6 d^{-1} (bottom line, Fig. 6b).

The NO_3^- mass removal increased linearly with the influent concentration during summer baseflow, and as a result there was no effect on percentage removal (Fig. 6c). These findings are consistent with the first-order decay approach employed in this study.

NO_3^- removal was negligible (7×10^{-5}%) during the single winter baseflow simulation that was performed (not shown). The stream reach is gaining during the winter due to higher groundwater levels compared to the summer, and even in the presence of in-stream weirs, this prevented channel water and thus NO_3^- from entering the sediment. These results are consistent with Azinheira et al. (2014), where no hyporheic exchange was observed during winter baseflow due to the gaining nature of the stream. The non-zero result is because there were a small number of model cells where the stream was losing, though there were far fewer than there were gaining cells and they had much lower magnitudes (i.e. 5 mm/d in a typical gaining cell vs. 10^{-3} mm/d in a typical losing cell).

3.3. Storm flow nitrate removal by inset floodplains

Under storm flow conditions, the inset floodplains were engaged, but the in-stream structures did not induce hyporheic flow. The latter is due to generally losing conditions during stormflow and negligible water surface drop over the structures (Azinheira et al., 2014). Under these conditions, NO_3^- removal was limited by inset floodplain residence time and first-order removal rates (i.e. NO_3^- removal is reaction or kinetics limited). Over the 90 m stream reach the model results indicated at most 0.7% removal of the influent NO_3^-. Unlike for baseflow conditions where reactions occurred in the hyporheic zone, NO_3^- removal in storm flows was not limited by the rate of exchange between the main channel and the reactive zone (in this case the inset floodplains).

NO_3^- removal increased linearly with first-order NO_3^- removal rate (Fig. 7a) and increased non-linearly with inset floodplain area (Fig. 7b). The highest percentage removal was achieved at the greatest removal rate and with installation of inset floodplains on both sides of the entire stream reach. Similar to the baseflow simulations, influent NO_3^- concentration had no effect on percentage NO_3^- removal, but did affect total mass removed (Fig. 7c).

The Manning's roughness coefficient was varied in the storm flow model to observe whether it made a substantial difference with regard to NO_3^- removal (Fig. 7d). There was no effect. This is probably because, while an increase in the inset floodplain friction would increase water and hence NO_3^- residence times on the inset floodplains, it would also reduce the amount of water and hence NO_3^- entering the inset floodplains from the main channel. These effects appear to have cancelled one another out.

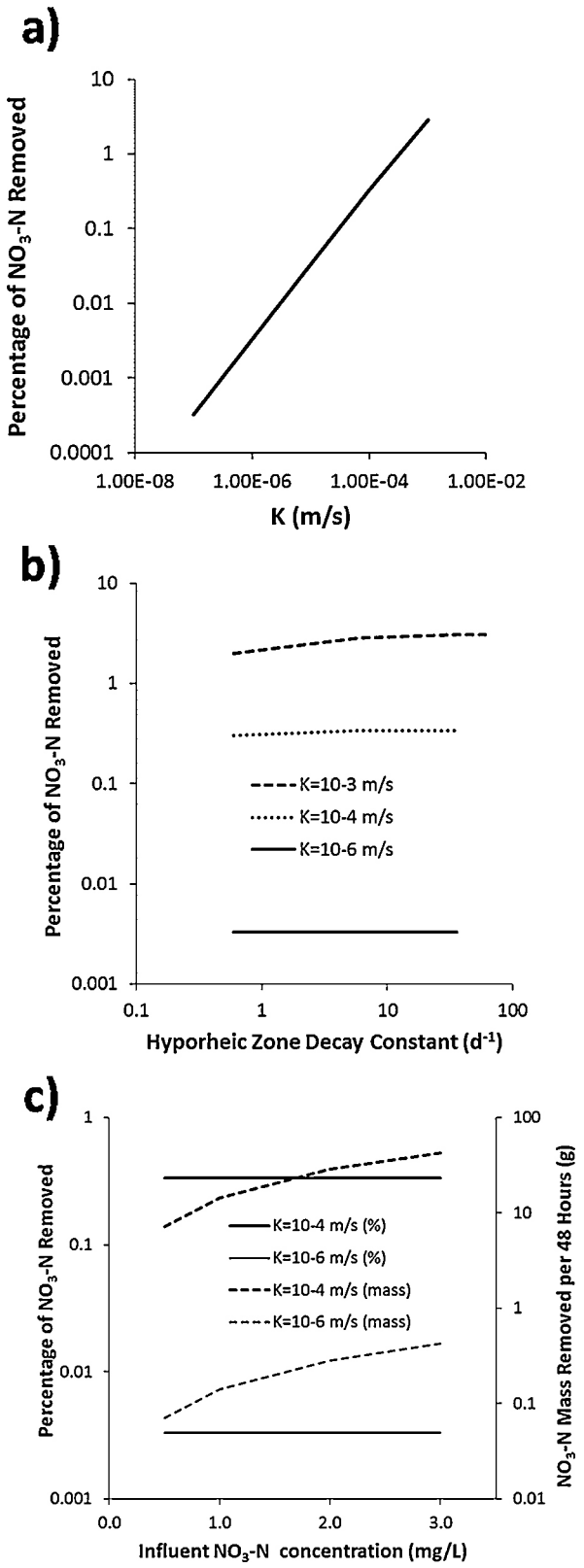

Fig. 6. Relationships between percent NO_3^- removal by structure-induced hyporheic exchange during summer baseflow conditions and a) streambed hydraulic conductivity for base case groundwater NO_3^- decay rate of 6 d^{-1}, b) first-order decay rate in the hyporheic zone, and c) influent NO_3^- concentration. 48-h NO_3^- mass removed is also included as a second dependent variable in panel c.

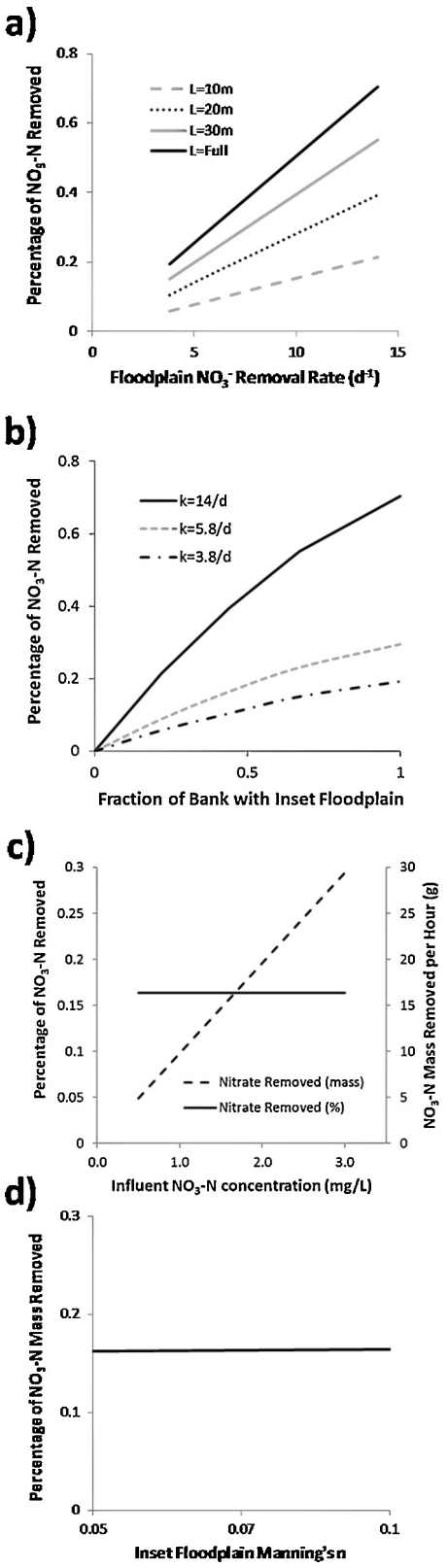

Fig. 7. Relationships between percent NO_3^- removal due to exchange with inset floodplains during storm flow conditions and a) first-order removal rate for different inset floodplain lengths (L), b) fraction of each bank with inset floodplains (F_b) for different first-order removal rates, c) influent NO_3^- concentration, and d) Manning's roughness coefficient in the inset floodplain. 1-h NO_3^- mass removed is also included as a second dependent variable in panel c.

4. Discussion and analysis

4.1. Controls on nitrate removal by structure-induced hyporheic flow and inset floodplains

Our results indicate that structure-induced hyporheic zones had greater potential for NO_3^- removal (up to 3%) in our 90 m reach than did inset floodplains (up to 0.7%) (Figs. 6–7). This comparison will likely hold for many restorations in channels of similar size and slope because we included the greatest density of in-stream structures possible given the channel slope (to prevent drowning of one structure by the next), and inset floodplains were continuous along the reach. Nevertheless, some modifications may affect these results, such as increasing the width (perpendicular to the channel) of the inset floodplains. Increasing the height of the in-stream structures would provide little additional effect as the structures would be drowned. Decreasing the height of the in-stream structures would allow more densely spaced structures, but the effect on NO_3^- removal is beyond the scope of our results and bears further study.

The results from our summer baseflow model show that NO_3^- removal from the hyporheic zone is limited by the rate of hyporheic exchange induced by the in-stream structures (transport limited). At hydraulic conductivities ranging from 10^{-4} to 10^{-7} m/s, hyporheic zone residence times were sufficiently long that all NO_3^- entering the hyporheic zone was removed, regardless of which first-order decay rate we chose. Only at $K = 10^{-3}$ m/s were residence times short enough that an increase in the decay rate from the minimum to the maximum value caused a non-trivial increase in NO_3^- removal.

At streambed hydraulic conductivities of 10^{-5} m/s or lower, the rate of hyporheic exchange was too low for significant NO_3^- removal (i.e. greater than 0.04% within the 90 m reach) to be achieved, regardless of the first-order decay rate. This suggests that streams with low- or even moderate-permeability beds would be poor candidates for stream restoration schemes that rely on hyporheic exchange.

Our storm flow model results indicate that inset floodplain residence time and first-order decay rate limit NO_3^- removal when the inset floodplains are inundated (reaction or kinetics limited). We observed linear increases in NO_3^- removal when we increased the rate and/or the inset floodplain area. Thus maximizing the length of inset floodplains is advised. Removal was not transport limited, in that far more NO_3^- was delivered to the inset floodplains than they were able to remove.

4.2. Comparison with Chesapeake Bay guidance

The Chesapeake Bay Program gives NO_3^- removal credits toward meeting the Chesapeake Bay Total Maximum Daily Load (TMDL) for various stream restoration activities (Berg et al., 2014), including In-Stream and Riparian Nutrient Processing within the Hyporheic Zone during Base Flow (Protocol 2) and Floodplain Reconnection Volume (Protocol 3). To our knowledge, these are unique worldwide in providing stream restoration water quality credit based on specific categories of restoration practice. We calculated the expected removal rates outlined in these protocols within Berg et al. (2014) for the 90 m reach of Stroubles Creek that we modeled, including the in-stream structures and inset floodplains. We then compared the expected removal rates to those predicted by our model.

We used Protocol 2 to estimate expected daily N removal in our 90 m modeled reach from structure-induced hyporheic flow during baseflow. We note that our approach for inducing nutrient removal via hyporheic transfer (i.e. in-stream structures that create potentiometric head gradients) is not mentioned in the Chesapeake Bay Program guidance. Rather, the guidance appears to focus on naturally occurring shallow hyporheic flowpaths and stream restoration design practices (e.g. filling the channel with cobbles and boulders) that may enhance them. Thus, our in-stream structures may be more aggressive than approaches espoused in Protocol 2.

Table 3
Comparison with Berg et al. (2014) Protocol 2.

Hydraulic Conductivity (m/s)	Influent NO_3^- Concentration (mg/L NO_3^-N)	Modeled Daily NO_3^- Removal (g/d NO_3^-N)	Berg et al. (2014) Daily NO_3^- (NO_3^-N) Removal (g/d)
10^{-4}	0.5–3	3.5–21	55
10^{-6}	0.5–3	0.035–0.21	

We calculated the volume of the subsurface hyporheic "box" according to the guidance (Berg et al., 2014) as 5 feet deep (1.52 m), as wide as the channel width plus 10 feet (3.05 m), and as long as that subset of the stream reach where there is evidence of hyporheic exchange. We used an average channel width of 3 m (approximately 3 1-m model cells) giving a box width of 6.05 m (20 ft). We calculated the box length by identifying the distance upstream of each structure where channel-to-groundwater water transfer was observed in the otherwise-gaining stream. We doubled this value at each structure (i.e. we assumed symmetrical hyporheic flow paths with respect to each structure), giving 56 m of stream reach with evidence of hyporheic exchange, and hence 56 m (184 ft) box length. This equates to a total hyporheic box volume of 520 m^3 (18,400 ft^3) with a total weight of 1.04×10^6 kg (1150 tons), based on a sediment bulk density of 2002 kg/m^3 (125 lbs/ft^3) (Berg et al., 2014). We multiplied 1150 tons by 1.06×10^{-4} lbs N/d/ton of soil (given in the guidance) to calculate a daily N removal volume of 55 g/d. We compared this to our summer baseflow results at $K = 10^{-4}$ m/s and $K = 10^{-6}$ m/s, with upstream NO_3^- concentrations ranging from 0.5 to 3 mg/L, and the base case first-order hyporheic NO_3^- decay rate of k = 6/d (Table 3).

Protocol 2 of Berg et al. (2014) estimates more daily N removal than the amount observed during our MIKE SHE model runs, especially at lower hydraulic conductivities. This is controlled by both hydraulic and sediment aspects, according to Darcy's Law. On the sediment side, the Protocol 2 hyporheic "box" approach does not consider the hydraulic conductivity of sediment, and therefore it is susceptible to overestimating N removal at sites with low hydraulic conductivity. On the hydraulic side, applications of Protocol 2 should be cautious not to overestimate the length of the hyporheic "box". Our MIKE SHE model indicated the length of hyporheic interaction was considerably less than the full channel reach length, yet practitioners might not always have access to a detailed model, and hyporheic flow patterns are not readily observable in the field (Hester and Gooseff, 2011). Also on the hydraulic side, denitrification from structure-induced hyporheic exchange requires hydraulic conditions that are not excessively gaining. This varies in time and space (see Section 4.4 below), yet this variation is not accounted for in the Chesapeake protocols. This emphasizes the variability of removal among sites based on variability of site conditions that are currently not accounted for in the Chesapeake protocols. Finally, removal rates calculated by Protocol 2 are zeroth order with respect to NO_3^- concentration, meaning the rate is flat regardless of inflowing concentration. By contrast, our approach was first order with respect to NO_3^- concentration, which is more in line with approaches typically taken in the scientific literature (Boyer et al., 2006; Stewart et al., 2011; Harvey et al., 2013; Zarnetske et al., 2015). This may mean that Protocol 2 may overestimate N removal at some concentrations and underestimate it at others.

Protocol 3 estimates NO_3^- load reduction as a function of the floodplain storage volume, expressed in units of watershed inches. Berg et al. (2014) provide removal curves for floodplain storage volumes ranging from 0.1 to 1 watershed inch. The inset floodplain storage volume for our modeled reach with full inset floodplains is 90 m length × 10 m width × 15 cm depth = 135 m^3, where the width includes the inset floodplains on both banks. This equates to only 3.5×10^{-4} watershed inches, because the inset floodplains are very small compared to the 15 km^2 watershed (Azinheira et al., 2014). Even if the storage depth in the floodplains is tripled beyond our modeled depth, and we assume that the entire 1.5 km restored reach of Stroubles Creek contains inset floodplains rather than just the modeled 90 m reach, the storage volume remains below 0.02 watershed inches.

The N removal curves provided by Berg et al. (2014) imply that near-zero floodplain storage volume (in watershed inches) yields near-zero total N removal. This is somewhat consistent with our model results, in that we also observed low (<1%) reach-scale N removal. The removals calculated from Berg et al. (2014) are even lower, though, as our inset floodplain storage volume does not even register on the Berg et al. (2014) charts. This suggests that even a 1.5 km inset floodplain installation at Stroubles Creek would be ineligible for N removal credits under Protocol 3, which is intended for floodplains with larger storage volumes (>0.1 watershed inches) relative to their respective watersheds.

In sum, this comparison of our model results with the Chesapeake Bay Program protocols suggests that Protocol 2 may overestimate N removal from hyporheic exchange, and that Protocol 3 requires very large floodplain inundation volumes (beyond those used in this study) to offer removal credits.

4.3. Extension to longer stream reaches

Our results indicate that when in-stream structures or inset floodplains are applied to a 90 m long stream reach, the magnitude of predicted water quality mitigation is typically minimal. The question then becomes whether stream restoration really needs to be a larger scale effort to achieve significant water quality benefit, perhaps viewed more as a watershed-scale effort. Modeling in-stream structures and inset floodplains along streams throughout a watershed stream network is beyond the scope of this study. However, we can provide a rough estimate of how much restoration effort would be needed at the watershed scale by estimating the length of a single contiguous restored reach that is needed to remove 30% of the inflowing NO_3^- mass during a storm flow or a period of summer baseflow. 30% is arbitrary, but a reasonable threshold based on Berg et al. (2014), who capped N removal estimates from hyporheic exchange and floodplain reconnection at 40% of daily load and approximately 16% of annual load, respectively. We performed the calculations for a variety of stream restoration scenarios. In each case we assumed that the entire restored reach would have the same characteristics as our 90 m modeled restored reach, and scaled up the estimated NO_3^- removal linearly with reach length. We recognize that streams will often not maintain the same characteristics across these longer reaches, but this exercise remains useful for order-of-magnitude understanding.

Results indicate that non-trivial NO_3^- reductions are possible, but achieving them may be more involved/expensive than expected based on Berg et al. (2014). The length of restoration required to meet a 30% removal threshold is highly variable depending on the hydraulic and reactive properties of the reach, and range from ~1 km to >800 km (Tables 4–5). Variability was highest for baseflow conditions, where hundreds of kilometers of restoration efforts are needed if hydraulic conductivity is relatively low ($K < 10^{-5}$ m/s). Even if the hyporheic zone were to have a high reaction rate it would not improve the rate of removal much (817 km compared to 819 km at $K = 10^{-6}$ m/s) because removal would be almost entirely transport-limited. By way of comparison, the stream segment of Stroubles Creek containing the modeled reach and extending downstream to the next major tributary (confluence with Wall Branch) is approximately ~8 km long (Wynn et al., 2010).

Table 4
Baseflow Reach Restoration Length Requirements.

Hydraulic Conductivity (K)	Hyporheic Zone Decay Rate (k)	Length of Restored Reach Required
10^{-3} m/s	36 d^{-1}	0.9 km
10^{-3} m/s	0.6 d^{-1}	1.4 km
10^{-4} m/s	36 d^{-1}	8.0 km
10^{-4} m/s	0.6 d^{-1}	9.0 km
10^{-6} m/s	36 d^{-1}	817 km
10^{-6} m/s	0.6 d^{-1}	819 km

Table 5
Storm Flow Reach Restoration Length Requirements.

Inset Floodplain Length	NO_3^- Uptake Rate	Length of Restored Reach Required
10 m	3.8 d^{-1}	46 km
10 m	14 d^{-1}	13 km
20 m	3.8 d^{-1}	26 km
20 m	14 d^{-1}	6.9 km
30 m	3.8 d^{-1}	18 km
30 m	14 d^{-1}	4.9 km
Full	3.8 d^{-1}	14 km
Full	14 d^{-1}	3.8 km

4.4. Extension in time (annual N reduction estimate)

In-stream structures and inset floodplains require that certain hydraulic conditions be met in order to remove NO_3^-. The inset floodplains are only engaged when they are inundated during storm events, and the in-stream structures only succeed in causing hyporheic exchange when background groundwater levels are sufficiently low (e.g., during summer baseflow). We used these facts to estimate the percent of inflowing NO_3^- mass that will be removed by the two restoration strategies throughout a year.

Azinheira et al. (2014) calculated that the inset floodplains were engaged approximately 1% of the year, and that in-stream structures induced hyporheic exchange approximately 20% of the year, in the restored reach of Stroubles Creek (Table 6, Column 2). We then took the NO_3^- mass removal percentages calculated from our MIKE SHE sensitivity analysis runs with full inset floodplains, the maximum inset floodplain N uptake rate, a streambed hydraulic conductivity of $K = 10^{-4}$ m/s, and the maximum hyporheic zone denitrification rate, and scaled them up to a 1 km reach (Table 6, Column 3). These conditions are again somewhat arbitrary, but they give a sense for the efficacy of these practices under fairly optimistic conditions. We then calculated how much NO_3^- mass flows into the model during each flow situation over the course of the year (Table 6, Column 4), and then the mass removal during each flow situation based on the removal percentages (Table 6, Column 5) by multiplying the two columns immediately to the left (Table 6, Columns 3 and 4).

Finally, we summed the total influent NO_3^- mass over the year and also the NO_3^- mass removal over the year, divided the two and multiplied by 100. This indicated that 2.1% of the total annual influent NO_3^- load would be removed during a full year. This is less than the removal rates that would be observed during a storm or during summer baseflow (7.9% and 3.7%, respectively, under these conditions) because during the rest of the year there is no NO_3^- removal because the inset floodplains are not engaged and the in-stream structures do not induce hyporheic exchange due to strong

Table 6
Annual Nitrate Removal from 1 km Reach.

Flow Situation	% of Year When Flow Situation Occurs (%, from Azinheira et al. (2014))	NO_3^- Percent Removal During Flow Situation (%)	Total Influent NO_3^- Mass During Flow Situation (kg, NO_3^-N)[1,2]	NO_3^- Mass Removal During Flow Situation (kg, NO_3^-N)
Summer Baseflow	20 (73 days)	3.7	$0.025\ m^3/s \times 1.5\ mg/L \times 73\ days = 237\ kg$	8.8
Storm Flow	1 (3.6 days)	7.9	$1.7\ m^3/s \times 1\ mg/L \times 3.6\ days = 529\ kg$	41.8
Rest of Year	79 (288 days)	0	$0.045^2\ m^3/s \times 1.5\ mg/L \times 288\ days = 1680\ kg$	0
Full Year	–	–	2446 kg	50.6

Note:

- We assumed that the storm flow NO_3^- concentration would be slightly lower (1 mg/L vs. 1.5 mg/L NO_3^-N) than the baseflow NO_3^- concentration for a given stream/watershed because of dilution (USGS, Undated).
- We estimated an average non-summer baseflow of 0.045 m^3/s using the summer (0.025 m^3/s) and winter (0.060 m^3/s) baseflow.
- Note that percent removal values in column 3 are higher than those shown in Figs. 6–7 because the sensitivity analysis that generated Figs. 6–7 was conducted one-at-a-time, i.e. all values were kept at base case values while each individual parameter was varied separately.

gaining conditions. It is fairly obvious that floodplains are only engaged during stormflow, but practitioners should be aware that hyporheic-exchange-inducing stream restoration techniques may also be engaged for only a certain fraction of the year, otherwise the strategy's efficacy will be overestimated.

4.5. Model limitations

Future work could improve upon our model to more comprehensively simulate NO_3^- transport and removal in the restored stream reach. For example, we assumed first-order removal of NO_3^- from the hyporheic zone based on prior work (Boyer et al., 2006; Stewart et al., 2011; Harvey et al., 2013; Zarnetske et al., 2015). As discussed earlier, this was a reasonable approximation given our relatively low NO_3^- concentrations. Nevertheless, denitrification can be more accurately modeled using Michaelis-Menten kinetics, therefore using a first-order simplification could overestimate NO_3^- removal at higher concentrations (e.g., >2 mg/L NO_3^-N).

Furthermore, within the groundwater saturated zone we assumed no nitrification in the presence of aerobic conditions (Gu et al., 2012), which would have added NO_3^- to the model rather than removing it. This is especially important at the high hydraulic conductivities (e.g., $K = 10^{-3}$ m/s), where hyporheic residence times may be too short to assume the prevalence of anaerobic conditions throughout the hyporheic flowpath. As discussed in the Methods section, this is reasonable when K is relatively low (10^{-4}–10^{-8} m/s) creating long residence times and negligible nitrification zones (Zarnetske et al., 2011; Marzadri et al., 2012). This also served as a better analog for many other anaerobic contaminant reactions which do not have precursor reactions (Hester et al., 2014).

While we were able to vary many parameters and boundary conditions during our analysis, we used just one particular stream reach with unchanging width and hydraulic radius. Some of our findings are likely applicable to many different streams, for example our observation that NO_3^- removal in the hyporheic zone was transport-limited whereas removal in the inset floodplains was kinetics-limited, but others might not be replicated at a different stream. For example, if our modeled reach were significantly wider relative to the depth, a greater percentage of the flow might move into the subsurface due to the in-stream structures and the percentage NO_3^- removal during summer baseflow might increase. Further analyses that vary the size and cross-sectional geometry of the channel would be required to assess the effectiveness of these two strategies in streams that are significantly different from our modeled reach.

For the storm flow model runs we assumed a certain rate of NO_3^- removal for all of the streamflow passing over the inset floodplains. We did not model the chemical interactions at the interface of the aqueous NO_3^- and the inset floodplain surface, instead opting to use floodplain-scale N removal data from a similar site. A more advanced model might implement the actual reactive zones at the surface and in the shallow subsurface of the inset floodplain (i.e. floodplain soils and plants) along with their respective properties that allow them to remove NO_3^- from water. However, we note that much of the data needed to support such a more detailed modeling approach is not yet available in the scientific literature, and thus this remains an important area for future research.

Finally, this model does not include NO_3^- originating in local groundwater or in runoff. As a result, we observed the effect of restoration practices on NO_3^- from upstream surface water sources in isolation. In other words, in our model, during summer baseflow, "clean" groundwater upwelled into the channel and caused reduction in concentration. We again note that this did not affect our quantification of percent or mass removal of NO_3^-originating in upstream surface water, but a more complete model would include these other possible NO_3^-sources. These are fertile areas for future research.

5. Conclusions

In our simulations we found that reach-scale NO_3^- removal from in-stream structures and inset floodplains is highly sensitive to changes in sediment conditions, biogeochemical parameters, and design parameters. Summer baseflow NO_3^- removal occurred due to structure-induced hyporheic exchange and thus depended mostly on streambed hydraulic conductivity. Hyporheic removal was transport limited except for $K > 10^{-4}$ m/s. By contrast, stormflow NO_3^- removal occurred due to inset floodplains and was controlled by inset floodplain length and N uptake rate in the floodplains. Hence floodplain removal was reaction or kinetics limited.

Although the Chesapeake Bay Program stream restoration guidance (Berg et al., 2014) does not include hydraulic conductivity when estimating hyporheic zone NO_3^- removal (Protocol 2), our results indicate that it was a critical parameter when assessing removal potential at our site. This may be one reason that Berg et al. (2014) estimates greater NO_3^- removal during summer baseflow (55 g/d for our 90 m modeled reach) than our results (0.035–21 g/d, depending on K and influent NO_3^- concentration). On the other hand, the Chesapeake Bay Program floodplain connection guidance (Protocol 3) did agree with our results in estimating very low (<1%) removals for our stream reach during storm flows.

Our model results indicate that NO_3^- reductions from in-stream structures and inset floodplains in a 90 m reach were generally minimal, not surpassing 3.1% during summer baseflow and 0.7% during storm flows under the most advantageous con-

ditions (i.e. $K = 10^{-3}$ m/s, full inset floodplain installation, and maximum hyporheic zone and inset floodplain reaction rates). In-stream structures were ineffective at hydraulic conductivities lower than $K = 10^{-4}$ m/s because very little NO_3^- entered the hyporheic zone relative to the amount flowing through the main channel. Non-trivial NO_3^- reductions likely require favorable sediment characteristics and/or stream restoration over several kilometers. For example, a 30% reduction in NO_3^- during storm flows required between 3.8 and 14 km of full inset floodplain installation in our model.

The difficulty in achieving significant NO_3^- reductions was exacerbated by temporally changing hydraulic conditions, as neither the in-stream structures nor the inset floodplains were engaged for the majority of the year. For example, a stream restoration scenario that removed 3.7% of the summer baseflow NO_3^- load and 7.9% of the storm flow NO_3^- load only removed 2.1% of the annual NO_3^- load. In sum, our model indicates that in-stream structures and inset floodplains can improve water quality, but overall required level of effort may be high to achieve desired results. The results from this study can be used when considering the suitability of each strategy at a given site.

Acknowledgements

This work was supported by the United States National Science Foundation (NSF) under grant NSF-ENG-1066817. The opinions expressed are those of the authors and not necessarily those of the NSF. Benjamin Hammond received support from the Charles E. Via Jr., Foundation in the Via Department of Civil and Environmental Engineering at Virginia Tech. The Danish Hydraulic Institute provided MIKE SHE at the discounted academic rate. Two anonymous reviewers provided helpful comments that improved the paper.

References

Azinheira, D.L., Scott, D.T., Hession, W.C., Hester, E.T., 2014. Comparison of effects of inset floodplains and hyporheic exchange induced by in-stream structures on solute retention. Water Resour. Res. 50, 6168–6190.

Berg, J., Burch, J., Cappuccitti, D., Filoso, S., Fraley-McNeal, L., Goerman, D., Hardman, N., Kaushal, S., Medina, D., Meyers, M., 2014. Recommendations of the Expert Panel to Define Removal Rates for Individual Stream Restoration Projects. Chesapeake Bay Program.

Bernhardt, E.S., Palmer, M.A., Allan, J.D., Alexander, G., Barnas, K., Brooks, S., Carr, J., Clayton, S., Dahm, C., Follstad-Shah, J., Galat, D., Gloss, S., Goodwin, P., Hart, D., Hassett, B., Jenkinson, R., Katz, S., Kondolf, G.M., Lake, P.S., Lave, R., Meyer, J.L., O'Donnell, T.K., Pagano, L., Powell, B., Sudduth, E., 2005. Ecology—synthesizing US river restoration efforts. Science 308, 636–637.

Boyer, E.W., Alexander, R.B., Parton, W.J., Li, C., Butterbach-Bahl, K., Donner, S.D., Skaggs, R.W., Del Gross, S.J., 2006. Modeling denitrification in terrestrial and aquatic ecosystems at regional scales. Ecol. Appl. 16, 2123–2142.

Brookes, A., Shields, F.D. (Eds.), 1996. River Channel Restoration: Guiding Principles for Sustainable Projects. John Wiley and Sons, Chichester, UK.

Buchanan, B.P., Walter, M.T., Nagle, G.N., Schneider, R.L., 2012. Monitoring and assessment of a river restoration project in central New York. River Res. Appl. 28, 216–233.

Calver, A., 2001. Riverbed permeabilities: information from pooled data. Ground Water 39, 546–553.

Cardenas, M.B., Cook, P.L.M., Jiang, H.S., Traykovski, P., 2008. Constraining denitrification in permeable wave-influenced marine sediment using linked hydrodynamic and biogeochemical modeling. Earth Planet. Sci. Lett. 275, 127–137.

Craig, L.S., Palmer, M.A., Richardson, D.C., Filoso, S., Bernhardt, E.S., Bledsoe, B.P., Doyle, M.W., Groffman, P.M., Hassett, B.A., Kaushal, S.S., Mayer, P.M., Smith, S.M., Wilcock, P.M., 2008. Stream restoration strategies for reducing river nitrogen loads. Front. Ecol. Environ. 6, 529–538.

Crispell, J.K., Endreny, T.A., 2009. Hyporheic exchange flow around constructed in-channel structures and implications for restoration design. Hydrol. Processes 23, 1158–1168.

DHI, 2011. MIKE SHE User Manual Volume 2: Reference Guide, Edited. Danish Hydraulic Institute.

Doll, B.A., Grabow, G.L., Hall, K.R., Halley, J., Harman, W.A., Jennings, G.D., Wise, D.E., 2003. Stream Restoration: A Natural Channel Design Handbook. NC Stream Restoration Institute, NC State University, Raleigh, NC.

Downs, P.W., Gregory, K.J., 2004. River Channel Management: Toward Sustainable Catchment Hydrosystems. Arnold Publishers, London, UK.

Dubrovsky, N.M., Burow, K.R., Clark, G.M., Gronberg, J., Hamilton, P.A., Hitt, K.J., Mueller, D.K., Munn, M.D., Nolan, B.T., Puckett, L.J., 2010. The Quality of Our Nation's Water: Nutrients in the Nation's Streams and Groundwater, 1992–2004. USGS Circular 1350. US Department of the Interior, US Geological Survey.

Ensign, S.H., Doyle, M.W., 2005. In-channel transient storage and associated nutrient retention: evidence from experimental manipulations. Limnol. Oceanogr. 50, 1740–1751.

Ensign, S.H., Doyle, M.W., 2006. Nutrient spiraling in streams and river networks. J. Geophys. Res. Biogeosci. 111.

Gordon, R.P., Lautz, L.K., Daniluk, T.L., 2013. Spatial patterns of hyporheic exchange and biogeochemical cycling around cross-vane restoration structures: implications for stream restoration design. Water Resour. Res. 49, 2040–2055.

Graham, D.N., Butts, M.B., 2005. Watershed models. Pages 245–272 Flexible, integrated watershed modelling with MIKE SHE.

Gu, C.H., Hornberger, G.M., Mills, A.L., Herman, J.S., Flewelling, S.A., 2007. Nitrate reduction in streambed sediments: effects of flow and biogeochemical kinetics. Water Resour. Res. 43.

Gu, C.H., Anderson, W., Maggi, F., 2012. Riparian biogeochemical hot moments induced by stream fluctuations. Water Resour. Res. 48.

Harvey, J.W., Bohlke, J.K., Voytek, M.A., Scott, D., Tobias, C.R., 2013. Hyporheic zone denitrification: controls on effective reaction depth and contribution to whole-stream mass balance. Water Resour. Res. 49, 6298–6316.

Henshaw, P.C., Booth, D.B., 2000. Natural restabilization of stream channels in urban watersheds. J. Am. Water Resour. Assoc. 36, 1219–1236.

Hester, E.T., Doyle, M.W., 2008. In-stream geomorphic structures as drivers of hyporheic exchange. Water Resour. Res. 44, W03417.

Hester, E.T., Gooseff, M.N., 2010. Moving beyond the banks: hyporheic restoration is fundamental to restoring ecological services and functions of streams. Environ. Sci. Technol. 44, 1521–1525.

Hester, E.T., Gooseff, M.N., 2011. Hyporheic restoration in streams and rivers. In: Simon, A., Bennett, S.J., Castro, J.M. (Eds.), Stream Restoration in Dynamic Fluvial Systems: Scientific Approaches, Analyses, and Tools. American Geophysical Union, Washington, DC.

Hester, E.T., Young, K.I., Widdowson, M.A., 2014. Controls on mixing-dependent denitrification in hyporheic zones induced by riverbed dunes: a steady state modeling study. Water Resour. Res. 50, 9048–9066.

Howarth, R.W., Sharpley, A., Walker, D., 2002. Sources of nutrient pollution to coastal waters in the United States: implications for achieving coastal water quality goals. Estuaries 25, 656–676.

Johnson, Z.C., Warwick, J.J., Schumer, R., 2015. A numerical investigation of the potential impact of stream restoration on in-stream N removal. Ecol. Eng. 83, 96–107.

Jones, C.N., Scott, D.T., Guth, C.R., Hester, E.T., Hession, W.C., 2015. Seasonal variation in floodplain biogeochemical processing in a restored headwater stream. Environ. Sci. Technol. 49 (22), 13190–13198.

Jordan, T., 2007. Wetland Restoration and Creation Best Management Practice (Agricultural). Definition of Nutrient and Sediment Reduction Efficiencies for Use in Calibration of the Phase 5.0 Chesapeake Bay Program Watershed Model. Smithsonian Environmental Research Center, Edgewater, MD.

Kasahara, T., Hill, A.R., 2006. Effects of riffle-step restoration on hyporheic zone chemistry in N-rich lowland streams. Can. J. Fish. Aquat.Sci. 63, 120–133.

Kaushal, S.S., Groffman, P.M., Mayer, P.M., Striz, E., Gold, A.J., 2008. Effects of stream restoration on denitrification in an urbanizing watershed. Ecol. Appl. 18, 789–804.

Kemp, W.M., Boynton, W.R., Adolf, J.E., Boesch, D.F., Boicourt, W.C., Brush, G., Cornwell, J.C., Fisher, T.R., Glibert, P.M., Hagy, J.D., Harding, L.W., Houde, E.D., Kimmel, D.G., Miller, W.D., Newell, R.I.E., Roman, M.R., Smith, E.M., Stevenson, J.C., 2005. Eutrophication of Chesapeake Bay: historical trends and ecological interactions. Mar. Ecol. Prog. Ser. 303, 1–29.

Kessler, A.J., Cardenas, M.B., Cook, P.L.M., 2015. The negligible effect of bed form migration on denitrification in hyporheic zones of permeable sediments. J. Geophys. Res. Biogeosci. 120, 538–548.

Landers, J., 2010. Entering the mainstream. Civil Eng. Mag. 2010 (August), 58–92.

Langland, M.J., Blomquist, J.D., Sprague, L.A., Edwards, R.E., 2000. Trends and Status of Flow, Nutrients, and Sediments for Selected Nontidal Sites in the Chesapeake Bay Watershed, 1985–98. US Department of the Interior, US Geological Survey. Open-File Report 99–451, Lemoyne, Pennsylvania.

Lautz, L., Fanelli, R., 2008. Seasonal biogeochemical hotspots in the streambed around restoration structures. Biogeochemistry 91, 85–104.

Leonard, B.P., 1979. A stable and accurate convective modelling procedure based on quadratic upstream interpolation. Comput. Methods Appl. Mech. Eng. 19, 59–98.

Marzadri, A., Tonina, D., Bellin, A., 2011. A semianalytical three-dimensional process-based model for hyporheic nitrogen dynamics in gravel bed rivers. Water Resour. Res. 47.

Marzadri, A., Tonina, D., Bellin, A., 2012. Morphodynamic controls on redox conditions and on nitrogen dynamics within the hyporheic zone: application to gravel bed rivers with alternate-bar morphology. J. Geophys. Res. Biogeosci. 117.

Mason, S.J.K., McGlynn, B.L., Poole, G.C., 2012. Hydrologic response to channel reconfiguration on silver bow creek, montana. J. Hydrol. 438, 125–136.

Menichino, G.T., Hester, E.T., 2014. Hydraulic and thermal effects of in-stream structure-induced hyporheic exchange across a range of hydraulic conductivities. Water Resour. Res. 50, 4643–4661.

NRCS, 2007. Stream Restoration Design, Part 654, National Engineering Handbook. USDA National Resources Conservation Service.
Opperman, J.J., Galloway, G.E., Fargione, J., Mount, J.F., Richter, B.D., Secchi, S., 2009. Sustainable floodplains through large-scale reconnection to rivers. Science 326, 1487–1488.
Palmer, M.A., Hondula, K.L., Koch, B.J., 2014. Ecological restoration of streams and rivers: shifting strategies and shifting goals. In: Futuyma, D.J. (Ed.), Annual Review of Ecology, Evolution, and Systematics, vol. 45, p. 247.
Roley, S.S., Tank, J.L., Stephen, M.L., Johnson, L.T., Beaulieu, J.J., Witter, J.D., 2012a. Floodplain restoration enhances denitrification and reach-scale nitrogen removal in an agricultural stream. Ecol. Appl. 22, 281–297.
Roley, S.S., Tank, J.L., Williams, M.A., 2012b. Hydrologic connectivity increases denitrification in the hyporheic zone and restored floodplains of an agricultural stream. J. Geophys. Res. Biogeosci. 117, G00n04.
Roni, P., Beechie, T.J., Bilby, R.E., Leonetti, F.E., Pollock, M.M., Pess, G.R., 2002. A review of stream restoration techniques and a hierarchical strategy for prioritizing restoration in Pacific northwest watersheds. North Am. J. Fish. Manage. 22, 1–20.
Roni, P., Bennett, T., Morley, S., Pess, G.R., Hanson, K., Van Slyke, D., Olmstead, P., 2006. Rehabilitation of bedrock stream channels: the effects of boulder weir placement on aquatic habitat and biota. River Res. Appl. 22, 967–980.
Rosgen, D.L., 2001. The cross-vane, W-Weir and J-Hook vane structures. Their description, design and application for stream stabilization and river restoration. In: Wetlands Engineering & River Restoration. American Society of Civil Engineers, Reno, Nevada, pp. 1–22, http://dx.doi.org/10.1061/40581(2001)72.
Royer, T.V., David, M.B., Gentry, L.E., 2006. Timing of riverine export of nitrate and phosphorus from agricultural watersheds in Illinois: implications for reducing nutrient loading to the Mississippi River. Environ. Sci. Technol. 40, 4126–4131.
Sheibley, R.W., Jackman, A.P., Duff, J.H., Triska, F.J., 2003. Numerical modeling of coupled nitrification-denitrification in sediment perfusion cores from the hyporheic zone of the Shingobee River, MN. Adv. Water Resour. 26, 977–987.
Stewart, R.J., Wollheim, W.M., Gooseff, M.N., Briggs, M.A., Jacobs, J.M., Peterson, B.J., Hopkinson, C.S., 2011. Separation of river network-scale nitrogen removal among the main channel and two transient storage compartments. Water Resour. Res. 47, W00j10.
Striz, E., Mayer, P.M., 2008. Assessment of Near-Stream Ground Water-Surface Water Interaction (GSI) of a Degraded Stream Before Restoration. EPA/600/R-07/058. U.S. Environmental Protection Agency.
USEPA, 2010. Chesapeake Bay Total Maximum Daily Load for Nitrogen, Phosphorus and Sediment. December 29, 2010. U.S. Environmental Protection Agency, Region 3.
USGS, Undated. Continuous Monitoring for Nitrate in USGS Water Science Centers Across the U.S. https://water.usgs.gov/coop/features/real-time.nitrate.summary.pdf Downloaded 5/19/2016.
Veraart, A.J., Audet, J., Dimitrov, M.R., Hoffmann, C.C., Gillissen, F., de Klein, J.J.M., 2014. Denitrification in restored and unrestored Danish streams. Ecol. Eng. 66, 129–140.
Wohl, E., Angermeier, P.L., Bledsoe, B., Kondolf, G.M., MacDonnell, L., Merritt, D.M., Palmer, M.A., Poff, N.L., Tarboton, D., 2005. River restoration. Water Resour. Res. 41, W10301.
Wohl, E., Lane, S.N., Wilcox, A.C., 2015. The science and practice of river restoration. Water Resour. Res. 51, 5974–5997.
Wynn, T., Hession, W.C., Yagow, G., 2010. Stroubles Creek Stream Restoration, Report 2007-WQIA-42. Virginia Dep. of Conserv. and Recreation and Virginia Tech Biol. Syst. Eng. Dep, Richmond,VA.
Zarnetske, J.P., Haggerty, R., Wondzell, S.M., Baker, M.A., 2011. Dynamics of nitrate production and removal as a function of residence time in the hyporheic zone. J. Geophys. Res. Biogeosci. 116, G01025.
Zarnetske, J.P., Haggerty, R., Wondzell, S.M., Bokil, V.A., Gonzalez-Pinzon, R., 2012. Coupled transport and reaction kinetics control the nitrate source-sink function of hyporheic zones. Water Resour. Res. 48, W11508.
Zarnetske, J.P., Haggerty, R., Wondzell, S.M., 2015. Coupling multiscale observations to evaluate hyporheic nitrate removal at the reach scale. Freshw. Sci. 34, 172–186.